Molecular reorganization energy in quantum-dot cellular automata switching EP

View Online   Export Citation   CrossMark

Subhash S. Pidaparthi[a] ID and Craig S. Lent ID

AFFILIATIONS

Department of Electrical Engineering, University of Notre Dame, Notre Dame, Indiana 46556, USA

[a]**Author to whom correspondence should be addressed:** subhash.pidaparthi@gmail.com

ABSTRACT

We examine the impact of the intrinsic molecular reorganization energy on switching in two-state quantum-dot cellular automata cells. Switching a bit involves an electron transferring between charge centers within the molecule. This, in turn, causes the other atoms in the molecule to rearrange their positions in response. We capture this in a model that treats the electron motion quantum-mechanically but the motion of nuclei semiclassically. This results in a non-linear Hamiltonian for the electron system. Interaction with a thermal environment is included by solving the Lindblad equation for the time-dependent density matrix. The calculated response of a molecule to the local electric field shows hysteresis during switching when the sweep direction is reversed. The relaxation of neighboring nuclei increases the localization of the electron, which provides an intrinsic source of enhanced bistability and single-molecule memory. This comes at the cost of increased power dissipation.

I. INTRODUCTION

Quantum-dot cellular automata (QCA) is a potential alternative to traditional complementary metal–oxide semiconductor (CMOS) transistor logic for nanoelectronics. QCA uses the configuration of localized charge to represent binary information.[1–9] A single mobile electron can be localized in a quantum dot, which is simply a region of space with a surrounding potential barrier that quantizes the charge enclosed. The arrangement of charge among multiple dots in a QCA cell encodes information and electron transfer (ET) between dots through quantum mechanical tunneling enables switching. The electric field from one cell influences neighboring cells enabling device operation. A two-dot cell captures the most basic elements of QCA operation. Three-dot or six-dot cells can support clocked control of the flow of information and allow power gain by replacing energy lost to dissipative processes through work done by the clock.

The QCA approach has been implemented in small metallic dots.[10] Logic gates including majority gates,[11] digital latches,[12] and shift registers[13,14] have been demonstrated. Power gain[15] and signal restoration have also been demonstrated in these systems.

Semiconductor QCA cells have been demonstrated in GaAs[16] and silicon[17] using dots formed by surface depletion gates. Another means of forming QCA cells in silicon is using a few implanted donor atoms to form the dots.[18] Molecular-scale QCA operation at room temperature has been achieved using dots formed by STM patterning of single dangling bonds on a hydrogen-passivated silicon surface.[19]

Achieving QCA operation using single molecules[20–22] has focused attention on the richly-studied field of mixed-valence chemistry. In these molecules, the role of dots is played by charge centers, frequently formed by metal atoms surrounded by coordinating ligands. The central metal atom can exist in more than one charge state and can be reversibly oxidized or reduced without breaking any chemical bonds. A second charge center within the molecule is connected through a bridging ligand so an electron can tunnel between dots. Of interest for QCA operation is the case when the charge centers are identical. If the bridging ligand presents a sufficient barrier to tunneling, the mobile charge will localize on one of the dots. The localization can be enhanced by the relaxation of the other atoms in a molecule in response to the presence or absence of the charge on one or the other dot.

A simple example of such a mixed-valence molecule is the diferrocenylacetylene (DFA)[23] molecule is shown in Fig. 1. In DFA, a pair of ferrocenyl groups is connected through a bridging ligand. The two iron centers act as the two dots where an electron can be localized.
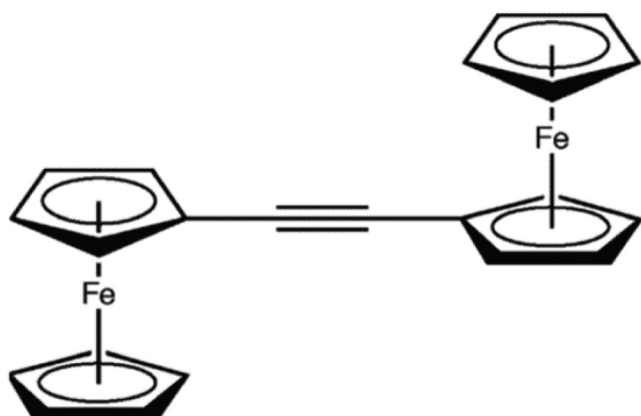
FIG. 1. Chemical structure of the mixed-valence diferrocenylacetylene (DFA) molecule. The iron centers in the two ferrocenyl groups act as dots for charge localization, forming a molecular double-dot. An extra electron present on one or the other dot encodes binary information. The energy associated with the relaxation of each ferrocenyl group in response to the presence or absence of the electron is the reorganization energy.

FIG. 2. Schematic representation of the effect of reorganization energy λ. A molecular double-dot can be viewed as a double potential well holding one mobile electron. If the electron is on the left (right) dot, the polarization is +1 (−1). Electron occupation of a dot induces a relaxation of the positions of the surrounding atoms in response. This relaxation lowers the energy of the occupied dot compared to the unoccupied dot by the reorganization energy λ.

The potential advantages of single-molecule devices of this type are several. The functional density could be enormous because the footprint of each molecule on the surface is of the order of a square nanometer. In reality, it would not be practical to separately address and control each molecule separately, so clocking schemes and appropriate computational architectures, such as a Kogge network,[24] would be necessary. Another advantage is that the intrinsic speed of such devices could be very high. Electron transfer in mixed-valence molecules can occur at picosecond timescales.[25] Finally, very low power dissipation may be possible because switching a bit requires only the motion of a single electron within the molecule. In contrast to molecular diodes or transistors, no current flow through the molecule is necessary.

Several candidate molecules for QCA have been synthesized and characterized. Fehlner et al. have synthesized QCA double-dots that were then covalently bonded to a semiconductor substrate.[26,27] They demonstrated controlled switching of the molecular charge between dots using external electrodes. The localization of charge in mixed-valence molecules has been imaged using STM.[28–31]

Most mixed-valence species are ions. This may present complications due to the presence of neutralizing counterions that could bias the charge configuration of the QCA molecule. One strategy is to include an electron donor (or acceptor) at a symmetric position within the molecule. This creates a neutral mixed-valence zwitterion.[32–34] Christie et al. have synthesized such a molecule, which could form the basis of a clockable three-dot QCA cell.[35]

Molecular QCA operation depends fundamentally on electric field driven ET between two dots within the molecule. We focus here on a simple model system that captures the essential features of this operation. Electron transfer in these systems is driven by an electric field, either produced by neighboring QCA molecules, or by clocking electrodes, or by input electrodes at the edges of a
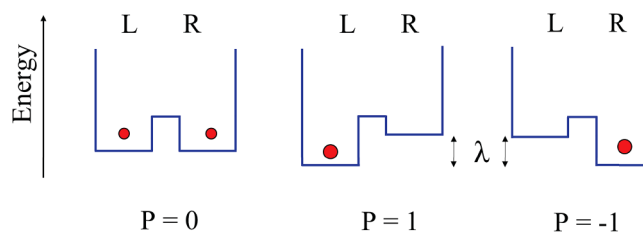
circuit array. This is in contrast to the usual situation in mixed-valence chemistry, where ET is produced by either the random motion of solvent molecules in solution or by incident light.

Full ab initio quantum chemistry calculations of molecular states are possible for the static problem in an electric field,[7,36–39] but the calculation of time-dependent switching dynamics are too costly and one must use reduced-state models that capture the relevant physics. The parameters of the simplified system can be taken from either quantum chemistry calculations or from experiments.

The key parameters for such a mixed-valence double dot system model are the inter-dot Hamiltonian tunneling matrix element, here called γ and often called H_{ab} in the chemical literature; the on-site energy difference due to the applied field, here called Δ; the Marcus reorganization energy λ that captures the effect of the nuclear relaxation due to charge occupancy of one or the other dot; the energy relaxation time T_d, which characterizes the energetic coupling between the molecule and the surrounding environment; and the environmental thermal energy $k_B T$.

The inter-dot tunneling energy γ determines the intrinsic time scale for the system and can be varied over 12 orders of magnitude by adjusting the bridging ligand.[25,40] Reference 31 shows the dramatic effect on the localization of simply altering the geometry of the connection between the dots and the bridging cyclopentadiene ring from the meta to para configuration.

A molecular double-dot can be simply modeled as a double potential well along the spatial axis connecting the two metal centers. (Note that this is not the Marcus double well as a function of the reaction coordinate). The reorganization energy λ lowers the energy of the occupied well compared to the unoccupied well due to the relaxation of other atoms, either those in the molecule itself or in the surrounding environment, as shown schematically in Fig. 2. The value of λ in solution can be affected by changing the solvent or by altering the chemical structure of the dot ligands. The reorganization energy can also be strongly affected by the attachment of the molecule to a surface. If the effective stiffness of the dot ligands is increased because of the constraint of the surface, the reorganization energy becomes smaller. (For a given force, a spring with a larger spring constant will store less energy than one with a smaller spring constant). A recent examination of the reorganization energy of a molecule with two ferrocene redox centers
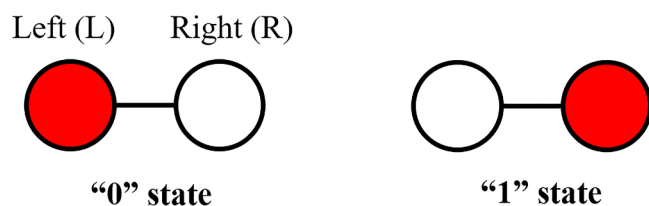
FIG. 3. Schematic of a two-state quantum-dot system. The black circles represent the quantum dots, the lines connecting the dots represent the inter-dot tunneling paths, and the red circles denote the localized charge. When charge is localized on the left dot (L), the system is in quantum state $|L\rangle$ and the polarization $P = 1$ represents a binary 0. When the charge is localized on the right dot (R), the system is in quantum state $|R\rangle$ and the polarization $P = -1$ represents a binary 1.

FIG. 4. Schematic representation of charge transfer during switching. At $t = 0$, the system is in the ground state and charge is localized on left dot L. Bias $\Delta(t)$ is applied to the left dot and is linearly increased from $\Delta_{initial}$ to Δ_{final} over the switching time T_s. Midway through the switching event at crossover $t = T_s/2$, the energies of the two dots are matched. At the end of the switching event $t = T_s$, charge is localized on the right dot and the electron transfer is complete.

connected by a naphthalene linker and deposited on a NaCl substrate showed reorganization energy in the few meV range, rather than the few hundred meV range for ferrocene in solution.[41,42] In a similar way, the strength of the coupling to the thermal environment, which determines T_d is dependent on the details of the surface attachment.

The reorganization energy λ can be obtained theoretically by high quality quantum chemistry calculations. The nuclear motion of all the atoms in the molecule that are coupled to the electron transfer can be expressed in terms of the normal modes of vibration. These can then be treated quantum mechanically, though again this is computationally costly because of the need to account for the harmonic oscillator degrees of freedom.[43,44]

We employ a parameterized Hamiltonian to describe the electron moving between the two charge centers under a driving field. The electron motion is linearly coupled to the nuclear reorganization via a single vibrational mode (the antisymmetric breathing mode). The energy transferred to the nuclear degrees of freedom is accounted for semiclassically so energy is conserved in the electron–vibron system. This leads to a nonlinear Hamiltonian for the electron degrees of freedom. Finally, the interaction with the thermal environment is included through Lindblad operators. Our focus is on accounting for the "self-trapping" aspect of the relaxation of nuclear coordinates associated with ET, the associated hysteresis in switching behavior, and the effect on power dissipation.

Low power dissipation for device switching is a key requirement for any nanoelectronics. For classical systems, the dissipated energy exhibits an inverse linear dependence on switching time ($1/T_s$). To calculate the energy dissipated for a quantum system, a first-order approach is to consider an isolated system and calculate the residual energy that remains in the system at the end of a switching event. This is the energy that will need to be eventually dissipated. For quantum switching, there is a remarkable exponential reduction[45] in the residual energy with switching time: $E \propto e^{-aT_s}$. For a rigid molecule, this has been extended to calculate dynamically the flow of energy between the molecule and the environment. For rapid switching, the power dissipation shows the characteristic quantum exponential decrease as the switching time is increased. For intermediate switching speeds, there is an inverted region in which power dissipation actually increases with a slower
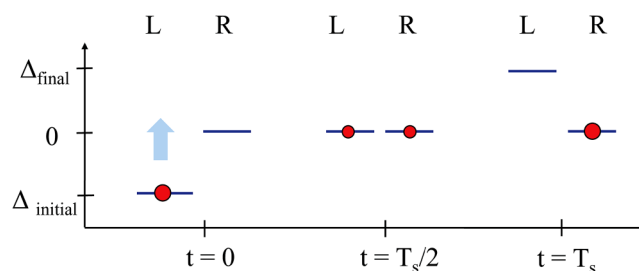
switching speed because of excitation from the thermal environment. At large switching times, the power dissipation follows the classical $1/T_s$ dependence.[46]

Here, we extend the model to include the effect of atomic reorganization. Section II describes the mathematical model for the system and interaction with the environment. Section III shows the impact of reorganization energy on polarization and switching dynamics. We solve the switching dynamically using the Lindblad equation and observe hysteresis in cell polarization when the bias sweep direction changes. Thus, we demonstrate that a single mixed-valence molecule can function as a memory element. In Sec. IV, we calculate the power dissipated by switching a bit. Higher reorganization energy causes an increase in dissipated power.

II. TWO-STATE MODEL

A two-state quantum-dot system is illustrated schematically in Fig. 3. It is the simplest QCA element consisting of two dots and a mobile charge. Charge transport between dots is through quantum-mechanical tunneling. We use $|L\rangle$ and $|R\rangle$ as the basis states, and the binary digital data in the two-state QCA is encoded in the polarization P. When the charge is fully localized on the left dot, the system is in state $|L\rangle$ and $P = 1$ representing a binary 0. When the charge is fully localized on the right dot, the system is in state $|R\rangle$ and $P = -1$ representing a binary 1.

Charge is transferred by changing the relative bias between the two dots. A simple switching operation is shown in Fig. 4. At $t = 0$, the charge is localized on the left dot. A time varying bias $\Delta(t)$ is applied to the left dot, and the right dot is held at 0. $\Delta(t)$ is linearly increased from $\Delta_{initial}$ to Δ_{final} over switching time T_s. Midway through the switching event at crossover $t = T_s/2$, the energies of the two dots are matched. At the end of the switching event $t = T_s$, if the bias Δ is large enough, the charge is almost entirely localized on the right dot and the electron transfer is complete. Polarization changes continuously from polarization $P = 1$ at $t = 0$ to polarization of $P = -1$ at $t = T_s$ in this example. We interpret polarization near 1 as a binary 0 and polarization near -1 as a binary 1.

The density operator $\hat{\rho}$ can be written in terms of Pauli operators as

$$\hat{\rho} = \frac{1}{2}(\hat{I} + \langle\hat{\sigma}_x\rangle\hat{\sigma}_x + \langle\hat{\sigma}_y\rangle\hat{\sigma}_y + \langle\hat{\sigma}_z\rangle\hat{\sigma}_z), \qquad (1)$$

where

$$\langle\hat{\sigma}_i\rangle = \mathrm{Tr}(\hat{\rho}\hat{\sigma}_i). \qquad (2)$$

The density operator is Hermitian with unit trace and the vector $(\langle\hat{\sigma}_x\rangle, \langle\hat{\sigma}_y\rangle, \langle\hat{\sigma}_z\rangle)$ will lie on or within a unit sphere (commonly called the Bloch sphere),

$$\sqrt{|\langle\hat{\sigma}_x\rangle|^2 + |\langle\hat{\sigma}_y\rangle|^2 + |\langle\hat{\sigma}_z\rangle|^2} \leqslant 1. \qquad (3)$$

The Hamiltonian operator for the simplified electronic two-state subsystem is written as

$$\hat{H}_E(t) = -\gamma\hat{\sigma}_x + \frac{\Delta(t)}{2}(\hat{\sigma}_z + \hat{I}). \qquad (4)$$

The characteristic time scale for dynamics is

$$T_\gamma = \frac{\pi\hbar}{\gamma}. \qquad (5)$$

The natural scales for the problem are to measure energy in units of γ and time in units of T_γ.

The polarization P is the expectation value of $\hat{\sigma}_z$,

$$P = \langle\hat{\sigma}_z\rangle = \mathrm{Tr}(\hat{\rho}\hat{\sigma}_z). \qquad (6)$$

When the electronic charge occupies a dot, the atoms around the dot shift their positions in response. This lowers the total energy for the electron being on that dot. The energy associated with this relaxation of nuclear positions is the reorganization energy of the Marcus theory λ.[47,48] The relaxation is modeled as the lowering of the energy of the dot when occupied by the electron (as in Fig. 2).

The Hamiltonian for linear coupling[49] between the electron and the motion of the surrounding ligands can be written in terms of λ:

$$\hat{H}_{EL} = -\frac{\lambda}{2}\hat{\sigma}_z\langle\hat{\sigma}_z\rangle. \qquad (7)$$

We treat the anti-symmetric oscillating motion of the left and right dot ligands as a classical harmonic driven by the imbalance between the electron occupancy between the left and right dots. The Hamiltonian operator representing this energy stored in the displaced ligand positions (classically $\frac{1}{2}kx^2$) is written as

$$\hat{H}_L = \frac{1}{2}(\frac{\lambda}{2})\langle\hat{\sigma}_z\rangle^2\hat{I}. \qquad (8)$$

Accounting in this way for energy as it moves back and forth between the electronic and vibrational degrees of freedom guarantees conservation of total energy.

The Hamiltonian is the sum of the Hamiltonians of the electronic subsystem $\hat{H}_E$, the electron-ligand interaction $\hat{H}_{EL}$, and the ligand subsystem $\hat{H}_L$:

$$\hat{H} = \hat{H}_E + \hat{H}_{EL} + \hat{H}_L. \qquad (9)$$

$$\hat{H} = -\gamma\hat{\sigma}_x + \frac{\Delta}{2}(\hat{\sigma}_z + \hat{I}) - \frac{\lambda}{2}\hat{\sigma}_z\langle\hat{\sigma}_z\rangle + \frac{1}{2}(\frac{\lambda}{2})\langle\hat{\sigma}_z\rangle^2\hat{I}. \qquad (10)$$

The Hamiltonian depends on the electron state through the expectation value $\langle\hat{\sigma}_z\rangle$. This non-linearity is fundamentally due to the fact that the effect of the ligand distortion on the electron system has been treated semiclassically.

When a system is in equilibrium with an environment at temperature T the steady-state density operator $\hat{\rho}_{ss}$ can be written as

$$\hat{\rho}_{ss} = \frac{e^{\frac{-\hat{H}(\hat{\rho}_{ss})}{k_BT}}}{\mathrm{Tr}(e^{\frac{-\hat{H}(\hat{\rho}_{ss})}{k_BT}})}. \qquad (11)$$

The steady-state Hamiltonian $\hat{H}_{ss} = \hat{H}(\hat{\rho}_{ss})$ depends on the steady-state density operator $\hat{\rho}_{ss}$ through Eq. (10). For given values of γ, Δ (which may vary in time), λ, and T, Eq. (11) must be solved self-consistently. We will see that in some circumstances, multiple solutions are possible for the same parameters.

For an isolated system, the time evolution of the density operator $\hat{\rho}$ is unitary and can be solved using the quantum Liouville equation

$$\frac{\partial\hat{\rho}}{\partial t} = \frac{1}{i\hbar}[\hat{H}(t), \hat{\rho}]. \qquad (12)$$

An open system interacts with the environment and the time evolution of the density operator is non-unitary. For Markovian systems, under reasonable assumptions, the density operator can be solved using a Lindblad equation[50–52]

$$\frac{\partial\hat{\rho}}{\partial t} = \frac{1}{i\hbar}[\hat{H}(t), \hat{\rho}] + \underbrace{\sum_k (\hat{L}_k\hat{\rho}\hat{L}_k^\dagger - \frac{1}{2}\{\hat{L}_k^\dagger\hat{L}_k, \hat{\rho}\})}_{\mathbb{D}}, \qquad (13)$$

where $\{\hat{A}, \hat{B}\}$ is the anti-commutator of operators $\hat{A}$ and $\hat{B}$. The first term in Eq. (13) governs the unitary evolution of the density operator and is identical to Eq. (12). The Lindblad dissipator $\mathbb{D}$ models the system–environment interaction including dissipation and decoherence. The $\hat{L}_k$ are the Lindblad operators. We model the coupling of the system to the thermal environment for our two-state system as

$$\hat{L}_1(t) = \sqrt{\frac{1}{T_d}}[|u_1(t)\rangle\langle u_2(t)|] \qquad (14)$$

$$\hat{L}_2(t) = \sqrt{\frac{1}{T_d}}, [e^{-\frac{E_2(t)-E_1(t)}{2k_BT}}|u_2(t)\rangle\langle u_1(t)|]. \qquad (15)$$

Here, $\hat{H}(t)|u_k(t)\rangle = E_k(t)|u_k(t)\rangle$, k_B is the Boltzmann constant, and T is the temperature of the environment (bath). T_d is a relaxation

time or dissipation time and is a measure of the coupling strength between the system and the environment. T_d is small for a system coupled strongly with the thermal bath. For an isolated system with no interaction with the environment, $T_d = \infty$ and both $\hat{L}_1$ and $\hat{L}_2$ are zero.

The Lindblad operator $\hat{L}_1$ in Eq. (14) models the decay of the system from the instantaneous excited state to the instantaneous ground state by dissipating energy to the environment. The Lindblad operator $\hat{L}_2$ in Eq. (15) models the thermal excitation of the system from the ground state to the excited state by absorbing thermal energy from the environment. The operators are constructed such that when the potential driver stops at $t = T_s$, the density operator will relax with characteristic time T_d to the thermal equilibrium density operator in Eq. (11).

III. POLARIZATION OF AN OPEN TWO-STATE SYSTEM DURING SWITCHING

A. Hysteresis in polarization during dynamic switching

We calculate the polarization during a switching operation of an open two-state system with a Hamiltonian defined in Eq. (10). We solve the Lindblad equation in Eq. (13) for the density operator $\hat{\rho}(t)$ as a function of time, and the polarization P is calculated directly from the density operator using Eq. (6). The system is in contact with the environment at temperature T, and the coupling between the system and environment is characterized by the dissipation time T_d. Initially at $t = 0$, the bias is $\Delta_{\min} = -25\gamma$, and the system is in equilibrium with the environment. The initial dot occupancy probabilities are determined by the steady-state density operator from Eq. (11). The bias is linearly increased from $\Delta_{\min} = -25\gamma$ at $t = 0$ to $\Delta_{\max} = +25\gamma$ over switching time $t = T_s$, which we define as a positive sweep. After the positive sweep, the bias is held at $\Delta_{\max}$ for a time sufficiently long such that the system can come to equilibrium with the environment. Then, the bias is linearly decreased from $\Delta_{\max}$ back down to $\Delta_{\min}$ over the same switching time T_s, which we define as a negative sweep. We explore the effect of changing the reorganization energy λ, switching time T_s, dissipation time T_d, and environmental temperature T.

Figure 5 shows the effect of the reorganization energy λ for quasi-adiabatic switching ($T_s/T_\gamma \gg 1$). When there is no reorganization energy ($\lambda = 0$), the polarization of the positive sweep and the negative sweep overlap. At zero bias ($\Delta = 0$), the polarization is zero, and, therefore, no binary information is stored in the two-state system.

When the reorganization energy is introduced, the system exhibits hysteresis. The polarization is different depending on the sweep direction. The hysteresis widens with increasing reorganization energy. At $t = T_s/2$ when the bias is zero ($\Delta = 0$), the polarization $P \approx 1$ or $P \approx -1$ depending on the sweep direction. This means the binary information ("0" bit or "1" bit) is stored even when the bias is removed. The polarization is closer to 1 or -1 when the reorganization energy increases indicating bit storage is easier at higher reorganization energies. We will discuss this more in Subsection III B. The slope of the polarization becomes more abrupt due to the effect of the
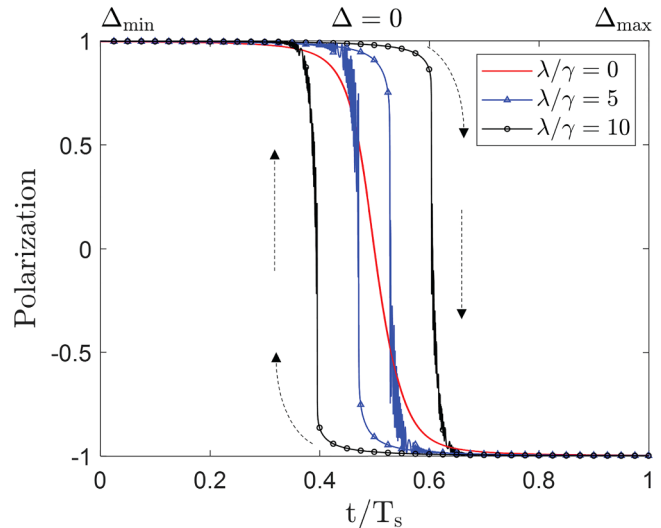

FIG. 5. Hysteresis in polarization and the impact of reorganization energy on an open system. Increasing reorganization energy λ increases the hysteresis in polarization and causes switching to be less gradual. With sufficient λ, polarization is approximately equal to +1 or -1 at zero bias ($t = T_s/2$) depending on the bias sweep direction. In this calculation, the bias Δ linearly increases from -25γ to $+25\gamma$ over switching time T_s during the positive sweep and decreases from $+25\gamma$ to -25γ over the same switching time T_s during the negative sweep. Here, $\lambda/\gamma = [0, 5, 10]$, $T_s = 1000T_\gamma$, $T_d = 10T_\gamma$, and $k_BT = 1\gamma$.

reorganization energy. The onsite energies of the left dot E_L and right dot E_R are defined as.

$$E_L(t) = \langle L|\hat{H}(t)|L\rangle \tag{16}$$

$$E_R(t) = \langle R|\hat{H}(t)|R\rangle. \tag{17}$$

In Fig. 6, we plot the difference of the onsite energies of the left and right dots ($E_L - E_R$) for the quasi-adiabatic switching calculations shown in Fig. 5. When $\lambda = 0$, $E_L - E_R$ simply matches the applied bias. The difference linearly increases from $\Delta_{\min}$ to $\Delta_{\max}$ during the positive sweep and linearly decreases from $\Delta_{\max}$ to $\Delta_{\min}$ during the negative sweep.

Now, consider the system with a nonzero reorganization energy. Initially, when charge is localized on the left dot ($P = 1$) the minimum value of $E_L - E_R$ is $\Delta_{\min} - \lambda$. During the positive sweep as the bias increases, $E_L - E_R$ increases at the same rate. When E_L comes closer to E_R, the charge transfer begins. Increasing charge occupation causes relaxation of the nuclei in the right dot and lowers the energy of right dot. The lowering of energy accelerates the charge transfer, which further lowers the energy of the right dot. This phenomenon causes switching to be less adiabatic and more abrupt. This is evident from the steeper slope of $E_L - E_R$ in a system with reorganization energy compared to a system with $\lambda = 0$. The polarization curves in Fig. 5 become abrupt with increasing reorganization energy. At the end of the positive sweep, the charge is localized on the right dot ($P = -1$), and $E_L - E_R$ is
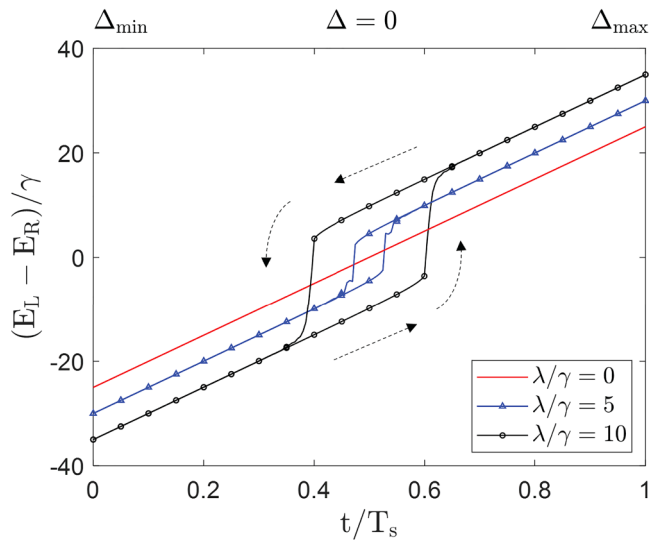
FIG. 6. Difference in onsite energy of dots $E_L - E_R$ for the switching operation shown in Fig. 5. With no reorganization energy $\lambda = 0$, $E_L - E_R$ matches the applied bias Δ. With a non-zero reorganization energy, the change in $E_L - E_R$ is faster (steeper slope) compared to the change in the applied bias. This causes the switching to be more abrupt and therefore less adiabatic.

FIG. 7. Hysteresis in polarization and the impact of switching time for an open system. For quasi-adiabatic switching (large T_s/T_γ), charge transfer is smooth and complete. Switching too rapidly causes quantum oscillations and incomplete charge transfer. The system may be left in the excited state at the end of the switching event. In this calculation, the bias Δ linearly increases from -25γ to $+25\gamma$ over switching time T_s during the positive sweep and decreases from $+25\gamma$ to -25γ over the same switching time T_s during the negative sweep. Here, $T_s/T_\gamma = [10, 100, 1000]$, $\lambda = 10\gamma$, $T_d = 10T_\gamma$, and $k_BT = 1\gamma$.

$\Delta_{\max} + \lambda$. The same behavior is observed during the negative sweep but in the opposite direction.

Figure 7 shows the impact of switching time T_s. When the switching is slow ($T_s/T_\gamma = 1000$), and, therefore, quasi-adiabatic switching, the system follows the instantaneous ground state in accordance with the adiabatic theorem. The charge switching is complete and the polarization changes from -1 to 1 and vice versa. When the switching is rapid (T_s/T_γ is small), the charge transfer is not complete at end of the sweep ($t = T_s$), and we observe charge quantum oscillations between the two dots post-crossover. The system will return to the ground state a sufficiently long time after the switching event.

Figure 8 shows the impact of coupling strength between the system and the environment. When the system is strongly coupled with the environment (T_d is small), any excess energy is immediately dissipated and the switching is more abrupt. For systems that are weakly coupled to the environment (T_d is large), the system takes longer to reach the ground state and the complete switching of the charge takes longer.

Figure 9 shows the impact of environmental temperature. At higher environmental temperature, the hysteresis decreases and the switching becomes less abrupt. The system takes longer to reach the ground state due to thermal excitation from the environment.

From Figs. 5 and 9, we observe that the width of the hysteresis is set by the reorganization energy λ and environmental temperature T. Changing either the switching time T_s or the dissipation time T_d (in Figs. 7 and 8), does not change the hysteresis but only changes the time taken to reach the steady state.
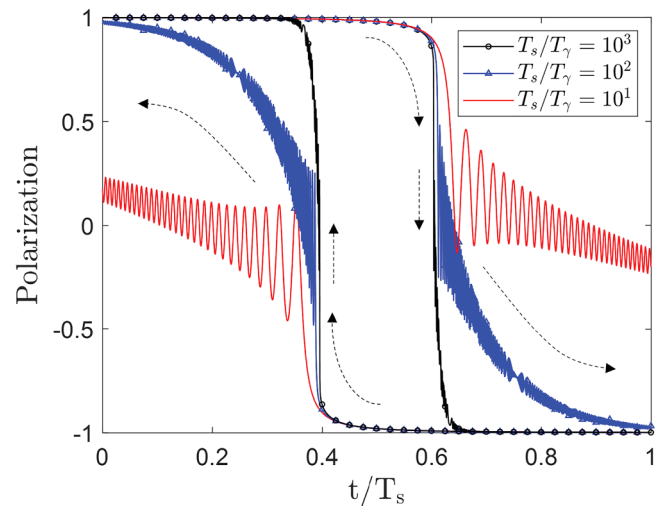
B. Memory operations on a two-state system with reorganization energy

The hysteresis observed in Fig. 5 shows that a system with nonzero reorganization energy can store a bit ("1" or "0") when the bias is zero during switching. We now perform a memory operation where we write and hold a "1" bit and then write and hold a "0" bit. The waveform of the applied bias is shown in Fig. 10(a), and the polarization response is shown in Fig. 10(b). We split this operation into four regions (I–IV) for the ease of explanation. Consider the polarization response when $\lambda = 5\gamma$.

In the region labeled I, the "1" bit is written. Initially at $t = 0$, the applied bias $\Delta = 0$ and the system is in equilibrium. The bias linearly increases and charge starts transferring. The bias is increased to $\Delta = +25\gamma$ by which point the charge is completely localized on the right dot with polarization $P = -1$. The system now represents a binary "1." The bias is then held constant for some time so the system can settle to a equilibrium. The bias is now linearly decreased from $\Delta = +25\gamma$ to $\Delta = 0$. In the system with significant reorganization energy ($\lambda = 5\gamma$), the charge does not transfer back and the polarization continues to be approximately -1. The binary information written into the system is locked. The bit is stored even when the bias is removed because the nuclear relaxation has localized the charge on the right dot.

In region labeled II, the bias is removed for a time duration of $10T_d$. The polarization for $\lambda = 5\gamma$ does not change significantly, and the binary information is not lost. The polarization continues to be approximately -1.
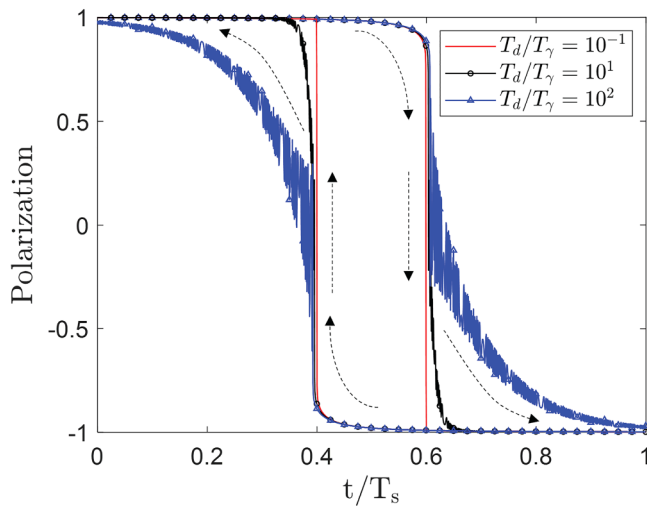
FIG. 8. Hysteresis in the polarization and the impact of coupling strength to the environment for an open system. Systems coupled strongly to the environment (small T_d) reach the steady state quickly. Weakly coupled systems (large T_d) take longer to reach the steady state. In this calculation, the bias Δ linearly increases from -25γ to $+25\gamma$ over switching time T_s during the positive sweep and decreases from $+25\gamma$ to -25γ over the same switching time T_s during the negative sweep. Here, $T_d/T_\gamma = [0.1, 10, 100]$, $T_s = 1000T_\gamma$, $\lambda = 10\gamma$ and $k_B T = 1\gamma$.
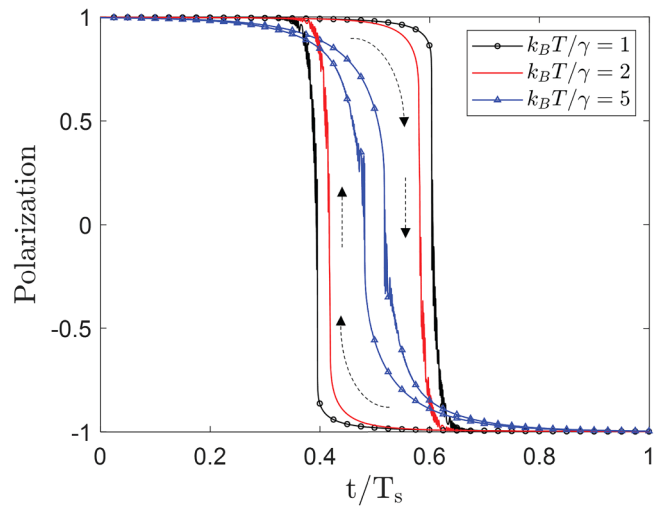

FIG. 9. Hysteresis in polarization and the impact of environmental temperature for an open system. Increasing temperature causes switching to be smoother and decreases hysteresis. In this calculation, the bias Δ linearly increases from -25γ to $+25\gamma$ over switching time T_s during the positive sweep and decreases from $+25\gamma$ to -25γ over the same switching time T_s during the negative sweep. Here, $k_B T/\gamma = [1, 2, 5]$, $T_s = 1000T_\gamma$, $T_d/T_\gamma = 10$, and $\lambda = 10\gamma$.

In the region labeled III, we write and hold a "0" bit, and, therefore, the applied bias is of opposite sign of the waveform in region I. The bias is decreased from $\Delta = 0$ to $\Delta = -25\gamma$, which causes the charge to localize on the left dot (P = 1), and the system now represents a binary "0." When the bias is increased from -25γ to back to 0, the polarization does not change significantly for $\lambda = 5\gamma$. The polarization continues to be approximately equal to 1.

In the region labeled IV, the bias is held at 0 for a time duration of $10T_d$ similar to region II. When $\lambda = 5\gamma$, the polarization continues to be approximately equal to 1 and the 0 bit is stored.

Figure 10 also shows the impact of reorganization energy. When $\lambda = 0$, there is no nuclear relaxation and the polarization is zero (bit not stored) in the absence of any applied bias. It is easier to hold binary information when the system has higher reorganization energy.

C. Multiple steady-state configurations

In Sec. III A, we calculated the polarization of a switching system dynamically using the Lindblad equation. We observed different values of polarization for the same value of applied bias. This means the system can be in more than one stable states. We now calculate the steady-state solutions of the system using Eq. (11) to determine under what circumstances the system will support a single or multiple equilibrium solutions.

We calculate the steady-state density operator $\hat{\rho}_{ss}$ at a given bias by self-consistently solving Eq. (11) using the constraint in Eq. (3). Without the loss of generality, we can set $\langle \hat{\sigma}_y \rangle = 0$. To solve
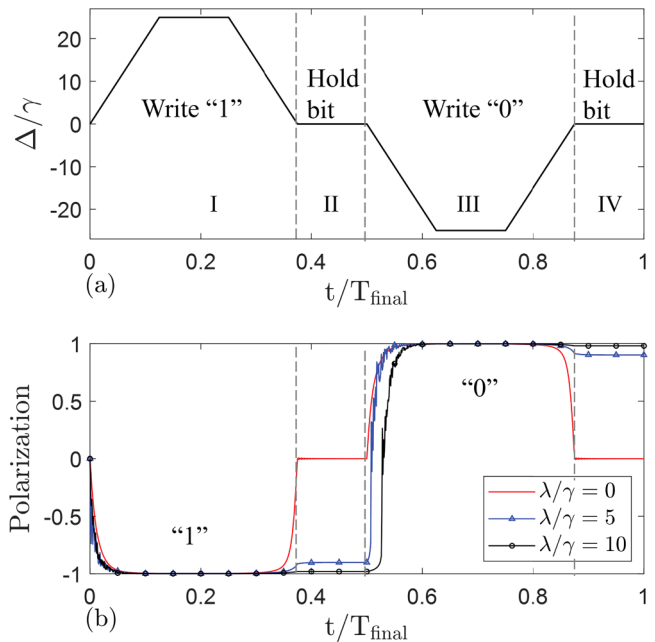

FIG. 10. Writing and holding 1 and 0 bits for different reorganization energy λ. In a system with sufficient reorganization energy, the polarization does not change significantly when the bias is removed. The system continues to store the bit (1 or 0) that is written. When $\lambda = 0$, the polarization becomes zero when the bias is removed and the bit is not stored. Here, $\lambda/\gamma = [0, 5, 10]$, $T_s = 1000T_\gamma$, $T_d = 10T_\gamma$, and $k_B T = 1\gamma$.
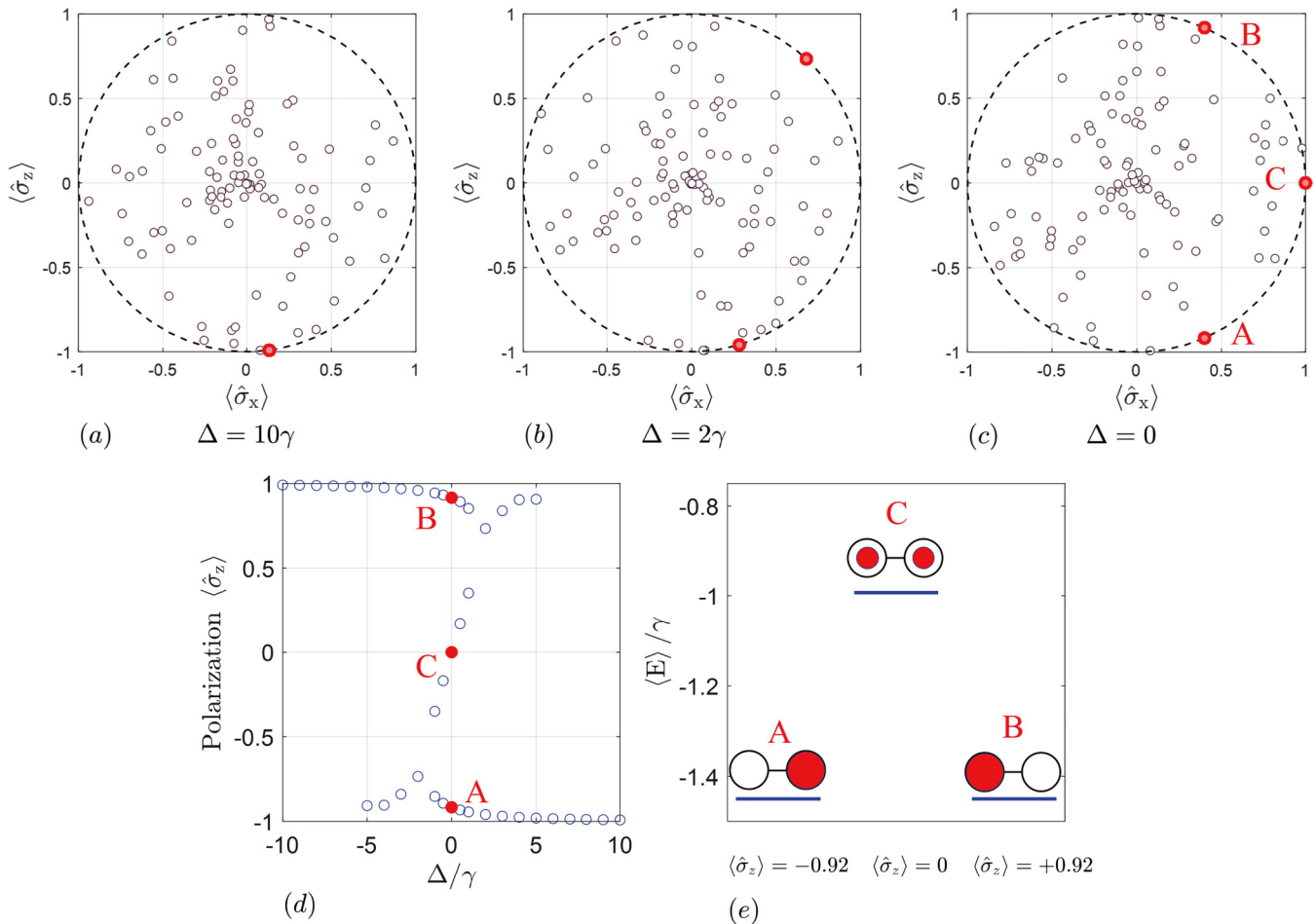
FIG. 11. Multiple equilibrium solutions of the density matrix for different applied biases. Solutions for the steady-state density operator $\hat{\rho}_{ss}$ are obtained by randomly choosing an initial state and solving Eq. (11) self-consistently for $\lambda = 5\gamma$ and $k_B T = 0.25\gamma$. In (a)–(c), the initial guesses are shown using open circle markers and steady-state solutions are show using filled circles. Steady-state solutions are calculated for three different bias values: (a) $\Delta = 10\gamma$. All initial guesses converge to a single steady-state solution. (b) $\Delta = 2\gamma$. There are two steady-state solutions, and the system is bistable. (c) $\Delta = 0$. There are three steady-state solutions which are labeled A, B, and C. (d) Steady-state polarization as a function of the applied bias. For small bias values, there are multiple steady-state solutions. (e) Expectation value of energy $\langle E \rangle$ for the three solutions A, B, and C at $\Delta = 0$ shown in (c) and (d). $\langle E \rangle$ for solutions A and B is lower than $\langle E \rangle$ for solution C. The result is that solution C is not visited during dynamic switching.

Eq. (11) iteratively, we start with an initial guess for the density operator and evaluate the RHS of Eq. (11) to obtain a value for $\hat{\rho}_{ss}$. This value is then substituted back into (11) and another iteration is obtained. These iterations continue until we obtain a converged solution for the density operator that satisfies Eq. (11). We then calculate the polarization from the steady-state density operator using Eq. (6).

We calculate the steady-state density operators for different values of bias Δ. Figures 11(a)–11(c) shows the results for bias $\Delta = 10\gamma$, 2γ, 0, respectively. Here, we take reorganization energy $\lambda = 5\gamma$ and environmental temperature $k_B T = 0.25\gamma$. The initial guess for the density operator is randomly chosen to lie on or within the unit circle defined by $\langle \hat{\sigma}_x \rangle$ and $\langle \hat{\sigma}_z \rangle$. We then solve Eq. (11) iteratively to obtain a converged steady-state solution for density

operator and $\langle \hat{\sigma}_x \rangle$ and $\langle \hat{\sigma}_z \rangle$. We perform this calculation for 100 random initial guesses for each bias condition by solving Eq. (11) for each of the initial guesses. In Figs. 11(a)–11(c), the random initial guesses are shown using open circles and the converged solutions for each of these initial guesses are shown using filled circles.

Figure 11(a) shows the results when the applied bias is large ($\Delta = 10\gamma$). After solving Eq. (11), all the initial random states yield a single solution for $\hat{\rho}_{ss}$ with a polarization $\hat{\sigma}_z = -0.99$ and the charge is localized on the right dot.

Figure 11(b) shows the results when the bias is lowered to $\Delta = 2\gamma$. All the initial random states converge to two possible solutions with polarization $\hat{\sigma}_z = -0.96$ and 0.73. The two polarization solutions are of opposite signs but not symmetric across zero. At a

low applied bias, the system is bistable. For these steady-state solutions, the majority of the charge can be localized on either dot.

Figure 11(c) shows the results when $\Delta = 0$. There are three possible steady-state solutions (labeled A, B, and C). Solutions A and B with $\langle \hat{\sigma}_z \rangle = -0.92$ and $\langle \hat{\sigma}_z \rangle = +0.92$ have the charge localized on the right or left dot, respectively. Solution C with $\langle \hat{\sigma}_z \rangle = 0$ has the charge equally distributed between the dots. At a bias value close to 0, there can be three steady-state solutions.

Figure 11(d) shows the steady-state polarization as a function of bias Δ. Multi-state equilibrium solutions are observed when the bias is comparable to $\lambda + k_B T$. The polarization curve exhibits hysteresis. There are solutions near the origin (example solution C) that are not observed in the hysteresis behavior during dynamic switching calculations in Fig. 5. To understand why, we calculate the expectation value of energy for solutions A, B, and C.

In Fig. 11(e), we calculate the expectation value of energy $\langle E \rangle$ for the three solutions A, B, C at $\Delta = 0$. $\langle E \rangle$ for the two symmetric solutions A and B are equal and $\langle E \rangle = -1.45\gamma$. For solution C, $\langle \hat{\sigma}_z \rangle = 0$ and the expected value of energy $\langle E \rangle = -0.99\gamma$. Solution C is not a stable state due to higher $\langle E \rangle$ compared to solutions A and B. Solution C will not be visited during dynamic switching. The system will select either solution A or B depending on the sweep direction.

IV. ENERGY DISSIPATION DUE TO SWITCHING

A. Isolated system

We can first calculate the energy dissipated by considering an isolated system, uncoupled from the environment, and then calculate the excess energy E_{excess} left in the system at the end of the switching event ($t = T_s$). We know that for an open system this is the energy that will be eventually dissipated. What this approach ignores is dissipation, or thermal excitation, that occurs to the environment during the switching process. For all calculations reported in this section, Δ is linearly increased -25γ to $+25\gamma$ over switching time T_s. This is sufficient to strongly localize the charge both before and after switching.

Consider the switching event described in Fig. 4. We define the excess energy of the system E_{excess} as the difference between the expectation value of the energy $\langle E \rangle$ and the ground state energy E_1 when the potential driver has stopped changing at $t = T_s$,

$$E_{excess} \equiv \langle E \rangle(T_s) - E_1(T_s). \quad (18)$$

The dimensionless adiabaticity parameter β captures the effect of the parameters that impact the adiabaticity of the switching

$$\beta \equiv \frac{2\pi\gamma^2 T_s}{\hbar|\Delta_{final} - \Delta_{initial}|}. \quad (19)$$

For an isolated system with no reorganization energy $\lambda = 0$, the excess energy E_{excess} decreases *exponentially* with β,

$$E_{excess} \approx \Delta_{final} e^{-\beta}. \quad (20)$$

There is no fundamental lower limit to E_{excess} as it can be decreased to any arbitrary low value by increasing the switching adiabaticity β.
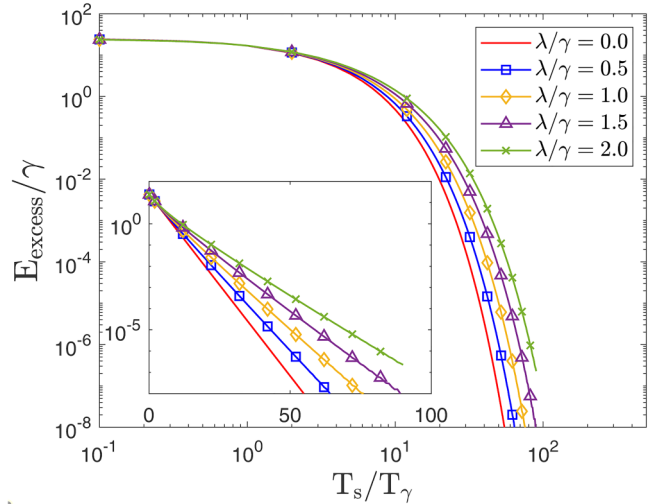

FIG. 12. Excess energy E_{excess} at the end of a switching event for an isolated system as a function of the switching time T_s for different values of the reorganization energy λ. The inset is the same data with the horizontal axis plotted on a linear scale. E_{excess} decreases exponentially with T_s when $\lambda = 0$. Increasing λ causes switching to be somewhat less adiabatic and increases E_{excess}.

The adiabaticity β can be made larger by switching more slowly (larger T_s), or using a smaller potential driver (smaller Δ), or by increasing γ.

The excess energy E_{excess} left in the system at the end of the switching event is calculated using Eq. (18) for different reorganization energies λ and plotted as a function of switching time T_s in Fig. 12. In the absence of reorganization energy $\lambda = 0$, E_{excess} decreases exponentially with increasing T_s (and therefore β) as shown in Eq. (20). This result has been discussed previously.[45] The excess energy increases with the introduction of a nonzero reorganization energy λ. The reorganization energy causes the switching to be less adiabatic (see explanation for Fig. 6 in Sec. III A). For the same switching speed, a system with higher reorganization energy has higher excess energy.

B. System in contact with a thermal environment

We now calculate E_{diss}, the total energy dissipated for a system in contact with a thermal environment due to a switching event. We first calculate the energy dissipated E_{switch} during switching from $t = 0$ to $t = T_s$. We do this by calculating the power flow and then integrating it over $t = 0$ to $t = T_s$.

The total power flow P_{total} into the system is the derivative of expected energy of the system

$$P_{total} = \frac{\partial \langle E \rangle}{\partial t} = \frac{\partial}{\partial t} \text{Tr}(\hat{\rho}\hat{H}) = \text{Tr}\left(\frac{\partial}{\partial t} \hat{\rho}\hat{H}\right), \quad (21)$$

$$P_{total} = \text{Tr}\left(\frac{\partial \hat{\rho}}{\partial t} \hat{H} + \hat{\rho} \frac{\partial \hat{H}}{\partial t}\right). \quad (22)$$

Using the Lindblad equation in Eq. (13), we can write

$$P_{total} = \text{Tr}\left(\left(\frac{1}{i\hbar}[\hat{H}, \hat{\rho}] + \mathbb{D}\right)\hat{H} + \hat{\rho}\frac{\partial \hat{H}}{\partial t} \right), \qquad (23)$$

$$P_{total} = \frac{1}{i\hbar}\text{Tr}([\hat{H}, \hat{\rho}]\hat{H}) + \text{Tr}(\mathbb{D}\hat{H}) + \text{Tr}\left(\hat{\rho}\frac{\partial \hat{H}}{\partial t}\right). \qquad (24)$$

The first term vanishes because of the cyclic property of the trace, and Eq. (24) reduces to

$$P_{total} = \text{Tr}(\mathbb{D}\hat{H}) + \text{Tr}\left(\hat{\rho}\frac{\partial \hat{H}}{\partial t}\right). \qquad (25)$$

By expanding the second term in the above equation using Eq. (9), we obtain

$$P_{total} = \underbrace{\text{Tr}(\mathbb{D}\hat{H})}_{P_1} + \underbrace{\text{Tr}\left(\hat{\rho}\frac{\partial \hat{H}_E}{\partial t}\right)}_{P_2} + \underbrace{\text{Tr}\left(\hat{\rho}\frac{\partial \hat{H}_{EL}}{\partial t}\right)}_{P_3} + \underbrace{\text{Tr}\left(\hat{\rho}\frac{\partial \hat{H}_L}{\partial t}\right)}_{P_4}. \qquad (26)$$

By substituting Eq. (7) in the third term in Eq. (26), we get

$$P_3 = \text{Tr}\left(\hat{\rho}\frac{\partial \hat{H}_{EL}}{\partial t}\right) = -\frac{\lambda}{2}\text{Tr}\left(\hat{\rho}\hat{\sigma}_z\frac{\partial \langle \hat{\sigma}_z \rangle}{\partial t}\right). \qquad (27)$$

So,

$$P_3 = -\frac{\lambda}{2}\frac{\partial \langle \hat{\sigma}_z \rangle}{\partial t}\langle \hat{\sigma}_z \rangle. \qquad (28)$$

Similarly, using Eq. (8), we obtain

$$P_4 = \frac{\lambda}{2}\langle \hat{\sigma}_z \rangle \frac{\partial \langle \hat{\sigma}_z \rangle}{\partial t}. \qquad (29)$$

The third term P_3 and fourth term P_4 in Eq. (26) cancel each other and, therefore, the total power flow into the system reduces to

$$P_{total} = \underbrace{\text{Tr}(\mathbb{D}\hat{H})}_{P_1} + \underbrace{\text{Tr}\left(\hat{\rho}\frac{\partial \hat{H}_E}{\partial t}\right)}_{P_2}. \qquad (30)$$

We identify the second term P_2 in Eq. (30) as the power flowing into the system due to work done by the time-varying control electrodes during switching,

$$P_{work} = \text{Tr}\left(\hat{\rho}\frac{\partial \hat{H}_E}{\partial t}\right). \qquad (31)$$

We identify the first term P_1 in Eq. (30) as the instantaneous power flow *into* the system from the environment. The power flowing *from* the system into the environment is obtained by

simply changing the sign

$$P_{switch} = -\text{Tr}(\mathbb{D}\hat{H}). \qquad (32)$$

The total energy dissipated *during* the switching event E_{switch} is the integral of instantaneous power dissipated P_{switch} during entire switching event from $t = 0$ to T_s,

$$E_{switch} = \int_0^{T_s} P_{switch}(t)dt = -\int_0^{T_s} \text{Tr}(\mathbb{D}\hat{H})dt. \qquad (33)$$

We now consider the residual excess energy E_{excess} left in the system when the potential driver stops at $t = T_s$. This residual excess energy will be dissipated after some time $t > T_s$. We define E_{excess} as the difference between the non-equilibrium expectation value of the energy and the steady-state expectation value at the end of the switching event,

$$E_{excess} = \langle E \rangle(T_s) - \langle E_{ss} \rangle(T_s), \qquad (34)$$

where

$$\langle E \rangle(T_s) = \text{Tr}(\hat{\rho}(T_s)\hat{H}(T_s)), \qquad (35)$$

$$\langle E_{ss} \rangle(T_s) = \text{Tr}(\hat{\rho}_{ss}(T_s)\hat{H}_{ss}(T_s)). \qquad (36)$$

The steady-state values of $\hat{\rho}_{ss}$ and $\hat{H}_{ss}$ are obtained by solving Eq. (11) self-consistently. The total energy dissipated E_{diss} is the sum of the energy dissipated during switching E_{switch} and excess energy E_{excess} left at the end of switching event, which is eventually dissipated to the environment,

$$E_{diss} = E_{switch} + E_{excess}. \qquad (37)$$

Substituting Eqs. (33), (34), (35), and (36) in the above equation, we obtain

$$E_{diss} = -\int_0^{T_s} \text{Tr}(\mathbb{D}\hat{H})dt \\ + \text{Tr}(\hat{\rho}(T_s)\hat{H}(Ts) - \hat{\rho}_{ss}(T_s)\hat{H}_{ss}(T_s)). \qquad (38)$$

For an open system, we solve for the density operator $\hat{\rho}$ using the Lindblad equation in Eq. (13). We then calculate the total dissipated energy E_{diss} using Eq. (38). E_{diss} is calculated as a function of switching time T_s for different reorganization energies λ. We first focus on the $\lambda = 0$ case shown in Fig. 13, which is our previously reported result.[46] The E_{diss} vs T_s behavior can be broken into three regimes.

First, the exponentially adiabatic regime at rapid switching (low T_s), which is labeled I. When the switching is rapid, there is significant excess energy E_{excess} left in the system at the end of the switching event and the amount of energy dissipated during switching E_{switch} is negligible. The total dissipated energy $E_{diss} \approx E_{excess}$ and decreases exponentially with switching time as shown in Eq. (20).
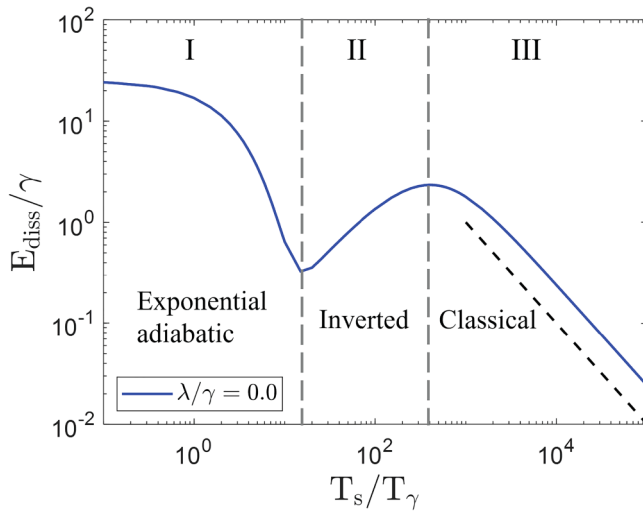
FIG. 13. Total dissipated energy E_{diss} of an open system as a function of switching time T_s with no reorganization energy ($\lambda = 0$). For rapid switching (small T_s) in the regime labeled I, E_{diss} exhibits exponential adiabaticity. For intermediate values of T_s in the regime labeled II, we observe the inverted region where E_{diss} actually increases as switching slows down. For large T_s in regime labeled III, E_{diss} follows the classical $1/T_s$ dependence. Here, the bias Δ is varied from -25γ to $+25\gamma$ over T_s, $T_d = 100T_\gamma$, and $kT = 3\gamma$. The dotted line simply indicates the slope of $1/T_s$ dependence on switching time that is characteristic of a classical system.

FIG. 14. Total dissipated energy E_{diss} of an open system as a function of switching time T_s for different reorganization energies λ. The $\lambda = 0$ calculation is the same as shown in Fig. 13. For small values of λ, E_{diss} is higher in the exponential adiabatic regime. E_{diss} is similar to E_{diss} for $\lambda = 0$ in the inverted and classical regimes. For larger values of λ, E_{diss} is increased in the exponential adiabatic region compared with the $\lambda = 0$ case and the inverted region vanishes. At higher T_s, E_{diss} shows a classical dependence on T_s. Here, the bias Δ is varied from -25γ to $+25\gamma$ over T_s, $T_d = 100T_\gamma$, and $kT = 3\gamma$. The dotted line is the $1/T_s$ dependence of a classical system.

Second, the inverted regime at intermediate switching speeds is labeled II. In this regime, we observe that the total dissipated E_{diss} increases as the switching speed decreases. It is surprising that slower switching produces higher dissipation. At these intermediate switching speeds, E_{excess} is negligible due to its exponential dependence on T_s. The total dissipated energy is approximately the energy dissipated during switching $E_{diss} \approx E_{switch}$. When the switching time is much faster than the dissipation time constant T_d, E_{diss} is small because the switching is complete before any thermal excitation from the environment can occur. As the switching speed slows down, thermal fluctuations from the environment cause excitations above the ground state. In this regime, the system is moving slowly enough for the excitations to occur but not slowly enough for them to immediately de-excite and permit the system to closely track the equilibrium occupations. The result is that slowing the switching speed counter-intuitively causes E_{diss} to increase. We have shown that the inverted region does not occur when environmental temperature is zero. The peak of the inverted region occurs at a switching time $T_s \approx 2T_d$. This inverted dependence has been confirmed using a semiclassical treatment.[46]

Third, the classical regime is labeled III at slow switching speeds (large T_s). Here, the total dissipated energy E_{diss} decreases linearly with T_s matching a classical system. At slow switching, the system is close to equilibrium with the environment and any thermal excitation or de-excitation occurs rapidly. But, the system is slightly excited and this energy decreases linearly with increasing switching time. The dotted line in Fig. 13 showing the $1/T_s$ dependence has been added as a visual guide.
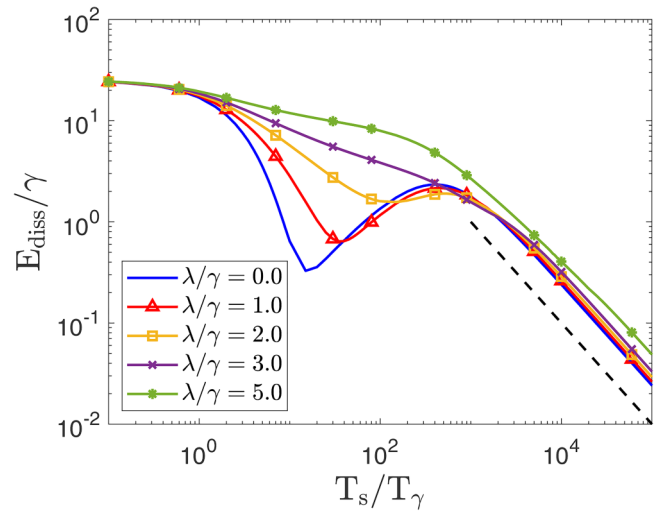
The impact of reorganization energy is shown in Fig. 14. When the reorganization energy is small ($\lambda/\gamma \lesssim 1$), we observe exponential dependence at rapid switching (small T_s). But, the rate of E_{diss} decrease is slower. At rapid switching, the dissipated energy is approximately equal to the excess energy left at the end of switching event $E_{diss} \approx E_{excess}$. This excess energy increases with increasing reorganization energy as shown in Fig. 12. As switching slows down, E_{diss} matches the system with no reorganization energy ($\lambda = 0$) and we observe the inverted region and the classical dependence.

At intermediate reorganization energies ($1 \lesssim \lambda/\gamma \lesssim 3$), the dissipated energy increases in the exponentially adiabatic region. At slower switching, E_{diss} meets the inverted dependence at $\lambda = 0$. The inverted region gets less pronounced with increasing reorganization energy.

At large reorganization energies ($\lambda/\gamma \gtrsim 3$), the dissipated energy is very high at rapid switching. At slower switching, the inverted region completely vanishes and the dissipated energy follows the classical $1/T_s$ dependence.

Figures 15 and 16 show the impact of environmental coupling when reorganization energy $\lambda = 1\gamma$ and $\lambda = 6\gamma$, respectively. T_d/T_γ is varied by four orders of magnitude from 10^{-1} to 10^3 at environmental temperature $k_B T = 3\gamma$. The dotted line shows the $1/T_s$ dependence of a classical system. When the system is very strongly coupled to the environment (T_d is small), any excess energy generated during switching is immediately dissipated and the system acts classically. The system does not exhibit the
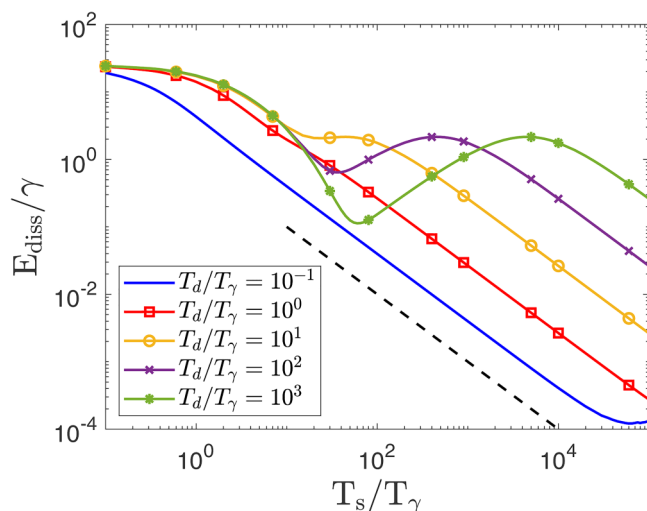
FIG. 15. Total dissipated energy E_{diss} of an open system as a function of switching time T_s for different values of the dissipation time constant T_d when the reorganization energy λ is small. Here, the bias Δ is varied from -25γ to $+25\gamma$ over T_s, $\lambda = 1\gamma$., and $kT = 3\gamma$. The dotted line is the $1/T_s$ dependence of a classical system.
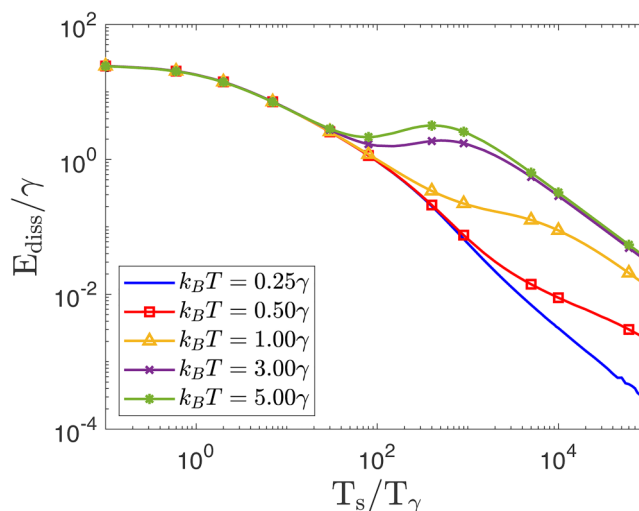

FIG. 17. Total dissipated energy E_{diss} of an open system as a function of switching time T_s for different values of the environmental temperature T. E_{diss} increases as T is increased. The inverted region becomes more pronounced with increasing T. Here, the bias Δ is varied from -25γ to $+25\gamma$ over T_s, $\lambda = 2\gamma$, and $T_d = 100T_\gamma$.

characteristic quantum adiabatic exponential decrease even at fast switching, which is evident in the $T_d/T_\gamma = 0.1$ case that shows E_{diss} linearly decreasing with T_s. For small reorganization energy, $\lambda = 1\gamma$ as the coupling becomes weaker, E_{diss} follows the
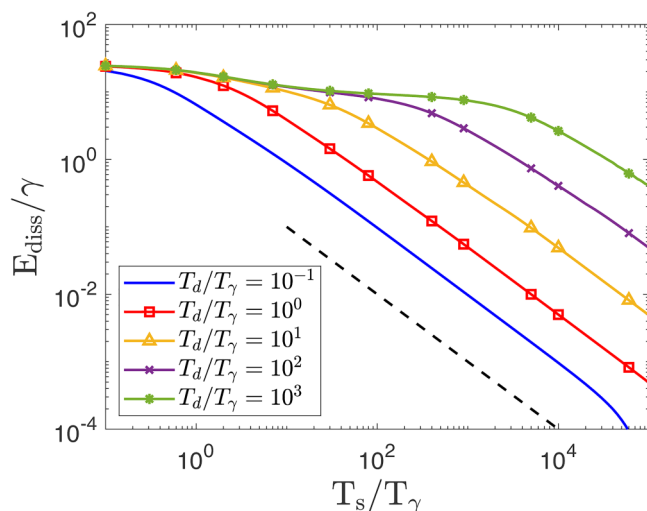

FIG. 16. Total dissipated energy E_{diss} of an open system as a function of switching time T_s for different values of the dissipation time constant T_d when the reorganization energy λ is large. Here, the bias Δ is varied from -25γ to $+25\gamma$ over T_s, $\lambda = 6\gamma$., and $kT = 3\gamma$. The dotted line is the $1/T_s$ dependence of a classical system.

exponential decrease of the isolated system at lower T_s, but eventually, as T_s increases, the interaction moves dissipation into the classical viscous regime. The inverted region between the two regimes is readily apparent. For larger reorganization energy $\lambda = 6\gamma$, E_{diss} decreases linearly with T_s and increases as environmental coupling weakens.

Figure 17 shows the results for different environmental temperatures with $T_d = 100T_\gamma$. We observe that when switching is rapid, E_{diss} matches the excess the energy of an isolated system. When the temperature is low there is no significant thermal excitation from the environment and E_{diss} decreases monotonically with T_s. As the temperature increases, E_{diss} starts exhibiting the inverted regime at larger switching times.

V. DISCUSSION

Molecular relaxation and subsequent lowering of dot energy upon charge occupation have been reported in candidate QCA molecules. We have here examined the impact of this molecular reorganization energy on the localization and energy dissipation of a two-state QCA cell.

The Hamiltonian of a QCA cell with reorganization energy, Eq. (10), is non-linear due to the effect of ligand distortion. The steady-state Hamiltonian depends on the steady-state density operator, and small applied biases can have multiple solutions for the same parameters, as seen in Fig. 11. We solved for the switching dynamics using the Lindblad Eq. (13) to model the environmental interaction at finite temperatures. Molecular QCA cells with non-zero reorganization energy display hysteresis in the polarization response, as shown in Fig. 9.

A stored memory bit must necessarily be in a long-lived meta-stable state that depends on the system's past. Because molecules cannot be addressed individually, the usual QCA approach is to hold binary information not in a single cell but rather in moving bit packets comprising several cells that are shepherded smoothly around a circuit by the clocking fields.[22,53] The device feature size can be much smaller than the electrodes that provide the clocking field which move information in computational waves around the circuit architecture.[24,54] The stability of the bit is then due to the large kinetic barrier to flipping all the cells in a bit packet, a stability which is enhanced by the quantum decoherence caused by the environment.[55]

The reorganization energy λ stabilizes the localized charge when the bias is removed, allowing a single molecular two-state QCA cell to act as a memory cell for storing a single bit. The molecular reorganization energy provides another source of bit stability, namely, the kinetic barrier associated with rearranging the atoms within the molecule in addition to moving the electron from site to site. The reorganization energy can be larger or smaller than $k_B T$, depending on the details of the molecule and its connection to the surrounding environment.

The enhanced bit stability due to the intrinsic molecular reorganization energy comes at the expense of somewhat higher power dissipation for a switching operation. As we have seen in Fig. 6, the movement of the dot ligands in response to the electron transfer accelerates the electron transfer process, in a way reminiscent of feedback. The result is lower adiabaticity and more energy dissipation for the same switching speed. It is to be noted that this effect is more pronounced at slower switching speeds than at higher speeds. If the switching speed is faster than the speed at which the ligands can respond, then the reorganization is irrelevant. For small reorganization energies, we observe three distinct regimes in dissipated energy dependence on switching time: an exponential adiabatic (e^{-aT_s}) regime, an inverted regime in which dissipation increases with slower switching, and a classical $1/T_s$ dependence for very slow switching. For large reorganization energy, the power dissipation is primarily classical.

From a practical molecular QCA design perspective, one has several key parameters to consider. The tunneling energy γ and, therefore, T_γ is determined by the choice of the linker between the charge centers. The coupling strength to the environment T_d depends on the precise way the molecule is bonded to substrate—essentially, the amount of heat-sinking. The switching signal E_c applied through electrodes and switching time T_s can be modified through the external driver circuitry. A mixed-valence molecule in a polar solvent typically has a large reorganization energy because many surrounding molecules must move to respond to an electron transfer event. For a surface-bound molecule not in solution, this energy can be much less. We have explored a range of λ in our calculations.

The results show a trade-off between enhanced QCA cell bi-stability and energy dissipation. One might expect that strong coupling to the environment, i.e., strong heat sinking (low T_d), would be optimal, but our results show otherwise. Systems with modest coupling to the substrate can take advantage of exponential adiabaticity at fast switching speeds (small T_s) and, therefore, optimize net power dissipation.

AUTHOR DECLARATIONS
Conflict of Interest

The authors declare no conflict of interest.

DATA AVAILABILITY

Data sharing is not applicable to this article as no new data were created or analyzed in this study.

REFERENCES

[1]C. Lent, P. Tougaw, W. Porod, and G. Bernstein, "Quantum cellular automata," Nanotechnology **4**, 49 (1993).
[2]P. D. Tougaw and C. S. Lent, "Logical devices implemented using quantum cellular-automata," J. Appl. Phys. **75**, 1818–1825 (1994).
[3]C. S. Lent and P. D. Tougaw, "A device architecture for computing with quantum dots," Proc. IEEE **85**, 541–557 (1997).
[4]C. S. Lent and P. D. Tougaw, "Bistable saturation due to single-electron charging in rings of tunnel-junctions," J. Appl. Phys. **75**, 4077–4080 (1994).
[5]A. Pulimeno, M. Graziano, A. Sanginario, V. Cauda, D. Demarchi, and G. Piccinini, "Bis-ferrocene molecular QCA wire: Ab initio simulations of fabrication driven fault tolerance," IEEE Trans. Nanotechnol. **12**, 498–507 (2013).
[6]M. Graziano, R. Wang, M. R. Roch, Y. Ardesi, F. Riente, and G. Piccinini, "Characterisation of a bis-ferrocene molecular QCA wire on a non-ideal gold surface," Micro Nano Lett. **14**, 22–27 (2019).
[7]R. Wang, A. Pulimeno, M. R. Roch, G. Turvani, G. Piccinini, and M. Graziano, "Effect of a clock system on bis-ferrocene molecular QCA," IEEE Trans. Nanotechnol. **15**, 574–582 (2016).
[8]A. Palii, S. Aldoshin, S. Zilberg, and B. Tsukerblat, "A parametric two-mode vibronic model of a dimeric mixed-valence cell for molecular quantum cellular automata and computational ab initio verification," Phys. Chem. Chem. Phys. **22**, 25982–25999 (2020).
[9]J. Modesto Clemente-Juan, A. Palii, E. Coronado, and B. Tsukerblat, "Mixed-valence molecular unit for quantum cellular automata: Beyond the Born-Oppenheimer paradigm through the symmetry-assisted vibronic approach," J. Chem. Theory Comput. **12**, 3545–3560 (2016).
[10]C. S. Lent and P. D. Tougaw, "Bistable saturation due to single-electron charging in rings of tunnel-junctions," J. Appl. Phys. **75**, 4077–4080 (1994).
[11]I. Amlani, A. O. Orlov, G. Toth, G. H. Bernstein, C. S. Lent, and G. L. Snider, "Digital logic gate using quantum-dot cellular automata," Science **284**, 289–291 (1999).
[12]A. O. Orlov, R. K. Kummamuru, R. Ramasubramaniam, G. Toth, C. S. Lent, G. H. Bernstein, and G. L. Snider, "Experimental demonstration of a latch in clocked quantum-dot cellular automata," Appl. Phys. Lett. **78**, 1625–1627 (2001).
[13]I. Amlani, A. O. Orlov, G. L. Snider, C. S. Lent, and G. H. Bernstein, "Demonstration of a six-dot quantum cellular automata system," Appl. Phys. Lett. **72**, 2179–2181 (1998).
[14]R. K. Kummamuru, A. O. Orlov, R. Ramasubramaniam, C. S. Lent, G. H. Bernstein, and G. L. Snider, "Operation of a quantum-dot cellular automata (QCA) shift register and analysis of errors," IEEE Trans. Electron Devices **50**, 1906–1913 (2003).
[15]R. K. Kummamuru, J. Timler, G. Toth, C. S. Lent, R. Ramasubramaniam, A. O. Orlov, G. H. Bernstein, and G. L. Snider, "Power gain in a quantum-dot cellular automata latch," Appl. Phys. Lett. **81**, 1332–1334 (2002).
[16]F. Perez-Martinez, I. Farrer, D. Anderson, G. A. C. Jones, D. A. Ritchie, S. J. Chorley, and C. G. Smith, "Demonstration of a quantum cellular automata cell in a GaAs/AlGaAs heterostructure," Appl. Phys. Lett. **91**, 032102 (2007).
[17]M. Macucci, M. Gattobigio, L. Bonci, G. Iannaccone, F. Prins, C. Single, G. Wetekam, and D. Kern, "A QCA cell in silicon-on-insulator technology: Theory and experiment," Superlattices Microstruct. **34**, 205–211 (2003).

[18]M. Mitic, M. C. Cassidy, K. D. Petersson, R. P. Starrett, E. Gauja, R. Brenner, R. G. Clark, A. S. Dzurak, C. Yang, and D. N. Jamieson, "Demonstration of a silicon-based quantum cellular automata cell," Appl. Phys. Lett. **89**, 013503 (2006).

[19]M. B. Haider, J. L. Pitters, G. A. DiLabio, L. Livadaru, J. Y. Mutus, and R. A. Wolkow, "Controlled coupling and occupation of silicon atomic quantum dots at room temperature," Phys. Rev. Lett. **102**, 046805 (2009).

[20]C. S. Lent, "Bypassing the transistor paradigm," Science **288**, 1597–1599 (2000).

[21]M. Lieberman, S. Chellamma, B. Varughese, Y. Wang, C. Lent, G. H. Bernstein, G. Snider, and F. C. Peiris, "Quantum-dot cellular automata at a molecular scale," Ann. N. Y. Acad. Sci. **960**, 225–239 (2002).

[22]C. S. Lent, B. Isaksen, and M. Lieberman, "Molecular quantum-dot cellular automata," J. Am. Chem. Soc. **125**, 1056–1063 (2003).

[23]J. A. Kramer and D. N. Hendrickson, "Electron transfer in mixed-valent diferrocenylacetylene and [2.2] ferrocenophane-1, 13-diyne," Inorg. Chem. **19**, 3330–3337 (1980).

[24]C. S. Lent, K. W. Henderson, S. A. Kandel, S. A. Corcelli, G. L. Snider, A. O. Orlov, P. M. Kogge, M. T. Niemier, R. C. Brown, J. A. Christie, N. A. Wasio, R. C. Quardokus, R. P. Forrest, J. P. Peterson, A. Silski, D. A. Turner, E. P. Blair, and Y. Lu, "Molecular cellular networks: A non von neumann architecture for molecular electronics," in *2016 IEEE International Conference on Rebooting Computing (ICRC), San Diego, CA, October 17–19, 2016* (IEEE, 2016).

[25]T. Ito, T. Hamaguchi, H. Nagino, T. Yamaguchi, J. Washington, and C. P. Kubiak, "Effects of rapid intramolecular electrontransfer on vibrational spectra," Science **277**, 660–663 (1997).

[26]H. Qi, S. Sharma, Z. H. Li, G. L. Snider, A. O. Orlov, C. S. Lent, and T. P. Fehlner, "Molecular quantum cellular automata cells. Electric field driven switching of a silicon surface bound array of vertically oriented two-dot molecular quantum cellular automata," J. Am. Chem. Soc. **125**, 15250–15259 (2003).

[27]J. Jiao, G. Long, F. Grandjean, A. Beatty, and T. Fehlner, "Building blocks for the molecular expression of quantum cellular automata: Isolation and characacterization of a covalently bonded square array of two ferrocenium and two ferrocene complexes," J. Am. Chem. Soc. **125**, 7522–7523 (2003).

[28]R. C. Quardokus, N. A. Wasio, R. P. Forrest, C. S. Lent, S. A. Corcelli, J. A. Christie, K. W. Henderson, and S. A. Kandel, "Adsorption of diferrocenylacetylene on Au(111) studied by scanning tunneling microscopy," Phys. Chem. Chem. Phys. **15**, 6973–6981 (2013).

[29]Y. Lu, R. Quardokus, C. S. Lent, F. Justaud, C. Lapinte, and S. A. Kandel, "Charge localization in isolated mixed-valence complexes: An STM and theoretical study," J. Am. Chem. Soc. **132**, 13519–13524 (2010).

[30]N. A. Wasio, R. C. Quardokus, R. P. Forrest, S. A. Corcelli, Y. Lu, C. S. Lent, F. Justaud, C. Lapinte, and S. A. Kandel, "STM imaging of three-metal-center molecules: Comparison of experiment and theory for two mixed-valence oxidation states," J. Phys. Chem. C **116**, 25486–25492 (2012).

[31]R. C. Quardokus, Y. Lu, N. A. Wasio, C. S. Lent, F. Justaud, C. Lapinte, and S. A. Kandel, "Through-bond versus through-space coupling in mixed-valence molecules: Observation of electron localization at the single-molecule scale," J. Am. Chem. Soc. **134**, 1710–1714 (2012).

[32]Y. Lu and C. S. Lent, "Counterion-free molecular quantum-dot cellular automata using mixed valence zwitterions—A double-dot derivative of the [closo-1-CB9H10]-cluster," Chem. Phys. Lett. **582**, 86–89 (2013).

[33]Y. Lu and C. Lent, "Self-doping of molecular quantum-dot cellular automata: Mixed valence zwitterions," Phys. Chem. Chem. Phys. **13**, 14928–14936 (2011).

[34]T. Groizard, S. Kahlal, and J.-F. Halet, "Zwitterionic mixed-valence species for the design of neutral clocked molecular quantum-dot cellular automata," Inorg. Chem. **59**, 15772–15779 (2020).

[35]J. A. Christie, R. P. Forrest, S. A. Corcelli, N. A. Wasio, R. C. Quardokus, R. Brown, S. A. Kandel, Y. Lu, C. S. Lent, and K. W. Henderson, "Synthesis of a neutral mixed-valence diferrocenyl carborane for molecular quantum-dot cellular automata applications," Angew. Chem. **127**, 15668–15671 (2015).

[36]Y. Lu and C. S. Lent, "A metric for characterizing the bistability of molecular quantum-dot cellular automata," Nanotechnology **19**, 155703 (2008).

[37]C. Lent, B. Isaksen, and M. Lieberman, "Molecular quantum-dot cellular automata," J. Am. Chem. Soc. **125**, 1056–1063 (2003).

[38]C. S. Lent and B. Isaksen, "Clocked molecular quantum-dot cellular automata," IEEE Trans. Electron Devices **50**, 1890–1896 (2003).

[39]Y. H. Lu, M. Liu, and C. Lent, "Molecular quantum-dot cellular automata: From molecular structure to circuit dynamics," J. Appl. Phys. **102**, 034311 (2007).

[40]R. A. Marcus, "Electron transfer reactions in chemistry: Theory and experiment," Rev. Mod. Phys. **65**, 599 (1993).

[41]J. Berger, M. Ondracek, O. Stetsovych, P. Maly, P. Holy, J. Rybacek, M. Svec, I. G. Stara, T. Mancal, I. Stary, and P. Jelinek, "Quantum dissipation driven by electron transfer within a single molecule investigated with atomic force microscopy," Nature Comm. **11**, 1337 (2020).

[42]A. Paul, R. Borrelli, H. Bouyanfif, S. Gottis, and F. Sauvage, "Tunable redox potential, optical properties, and enhanced stability of modified ferrocene-based complexes," ACS Omega **4**, 14780–14789 (2019).

[43]X. Yang and E. R. Bittner, "Intramolecular charge-and energy-transfer rates with reduced modes: Comparison to Marcus theory for donor–bridge–acceptor systems," J. Phys. Chem. A **118**, 5196 (2014).

[44]E. P. Blair, S. A. Corcelli, and C. S. Lent, "Electric-field-driven electron-transfer in mixed-valence molecules," J. Chem. Phys. **145**, 014307 (2016).

[45]S. Pidaparthi and C. Lent, "Exponentially adiabatic switching in quantum-dot cellular automata," J. Low Power Electron. Appl. **8**, 30 (2018).

[46]S. S. Pidaparthi and C. S. Lent, "Energy dissipation during two-state switching for quantum-dot cellular automata," J. Appl. Phys. **129**, 024304 (2021).

[47]R. A. Marcus, "Electrostatic free energy and other properties of states having nonequilibrium polarization. I," J. Chem. Phys. **24**, 979–989 (1956).

[48]R. A. Marcus, "On the theory of oxidation-reduction reactions involving electron transfer," J. Chem. Phys. **24**, 966–978 (1956).

[49]S. B. Piepho, E. R. Krausz, and P. N. Schatz, "Vibronic coupling model for calculation of mixed valence absorption profiles," J. Am. Chem. Soc. **100**, 2996–3005 (1978).

[50]H.-P. Breuer, F. Petruccione et al., *The Theory of Open Quantum Systems* (Oxford University Press, 2002).

[51]G. Lindblad, "On the generators of quantum dynamical semigroups," Commun. Math. Phys. **48**, 119–130 (1976).

[52]V. Gorini, A. Kossakowski, and E. C. G. Sudarshan, "Completely positive dynamical semigroups of n-level systems," J. Math. Phys. **17**, 821–825 (1976).

[53]C. Lent and B. Isaksen, "Clocked molecular quantum-dot cellular automata," IEEE Trans. Electron Devices **50**, 1890–1896 (2003).

[54]E. P. Blair, M. Liu, and C. S. Lent, "Signal energy in quantum-dot cellular automata bit packets," J. Comp. Theor. Nanosci. **8**, 972–982 (2011).

[55]E. P. Blair and C. S. Lent, "Environmental decoherence stabilizes quantum-dot cellular automata," J. Appl. Phys. **113**, 124302 (2013).